

Investigating allosteric communication with local search paths on protein residue networks

Susan Khor
slc.khor@gmail.com
(Date: Jan 19, 2016)

Abstract

We compare paths constructed on protein residue networks via a Euclidean Distance Search (*EDS*) to paths found using the commonly used Breadth First Search (*BFS*) method in terms of their ability to capture allosteric communication within proteins. We find that *EDS* paths are more stable and have better communication propensity than *BFS* paths. Further, *EDS* paths outperformed *BFS* paths at capturing key features of allosteric communication in a type III receptor tyrosine kinase (*KIT*), and at identifying protein sequence segments where known mutational hotspots are found. These findings suggest that *EDS* paths are more plausible discrete models of intra-protein communication pathways than *BFS* paths.

1. Introduction

Mapping out sites, regions and pathways within protein molecules that are functionally critical is an active area of research with important implications for drug delivery and for understanding the mechanics of molecular machines. To date, detailed studies of individual proteins or family of proteins to uncover such maps have been conducted using a combination of computational techniques and time intensive molecular dynamics (*MD*) simulation [1-4]. Less computationally demanding but more general studies have also been attempted by applying graph algorithms and complex network concepts to analyze crystallized protein structures represented as a network of interacting residues [5-7]. Such networks go by several names in the literature; we will call such a network, as defined in section 2.1, a Protein Residue Network or *PRN*.

In [8] we observed that paths constructed on the *PRN* of 166 proteins via the *EDS* algorithm (defined in section 2.2) possess several attractive properties over the shortest paths method (*BFS*) in terms of being more plausible intra-protein communication pathways. *EDS* is a greedy Euclidean distance Directed Search algorithm with backtracking similar in principal to Kleinberg's [9] local search algorithm. Efficient long-range intra-protein communication underpins allosteric interactions between cooperative binding sites which are crucial for proteins to be functional. *EDS* paths are more varied in length, are less diffusive (have lower search cost) and tend to make less use of long-range links [8]. These properties align with the anisotropic and sub-diffusive nature of allosteric communication in proteins [10], and experimental evidence that secondary structures play a major role in intra-protein energy transport [11]. Long-range links in a *PRN* are links between residues which are far apart (> 10) on the protein sequence but close to each other in the tertiary structure, and the cutoff of 10 residues means that most long-range links are links between rather than within secondary structures [12].

The properties of *EDS* paths mentioned above are rather general network properties. In this paper, we conduct a more specific investigation of *EDS* paths using measures taken directly from protein literature, namely stability and communication propensity, which are defined in section 2. We find that *EDS* paths are significantly more stable and have better communication propensity than *BFS* paths. This finding is a consequence of *EDS* paths' weaker affinity for long-range links previously observed in [8].

We also compare *EDS* paths with *BFS* paths in terms of their ability to capture key allosteric communication characteristics of a type III receptor tyrosine kinase (*RTK*), *KIT*. Kinase proteins play a major role in signal transduction by turning cellular signaling pathways on and off through phosphorylation of substrate proteins. Some kinases are self-activating. For *KIT*, this happens when its extra-cellular ligand-binding domains bind with stem cell factor (*SCF*) [13] which results in phosphorylation of its tyrosine residues (Fig. 1 in [14]). *KIT* can also be activated through point mutations, and such abnormal regulation of *KIT* has been implicated in several cancers.

The key allosteric characteristics of KIT that we will be examining are based on the study by Laine et al. [2]. In that study, allosteric communication in the cytoplasmic region of KIT (PDB: 1T45, chain A, residues 547...694, 753...935) was derived from MD simulations and represented as a network of *independent dynamic segments* (IDSs) connected by *communication pathways* (CPs). IDSs and CPs are described in more detail in section 2. This network representation was sensitive enough to detect differences between KIT in its wild-type (WT) form which is inactive or auto-inhibited, and the active form of KIT induced by an oncogenic point mutation, D816V (aspartate at position 816 is replaced with valine). In WT, at least one CP connects the juxtamembrane region (JMR, residues 547...581) to the spatially distant activation loop region (A-loop, residues 810...835) via the catalytic-loop (residues 790...797). This CP disappears when WT is activated by D816V, which triggers structural reorganization of the JMR and A-loop regions, and decreases communication between the N- and C- lobes of the protein kinase domain (PTK) of KIT. This change in communication pattern reflects the repositioning of the JMR in relation to the PTK. The JMR is more detached from the PTK when KIT is active. Communication between JMR and A-loop via the catalytic-loop is restored with a second point mutation, D792E (aspartate at position 792 is replaced with glutamate), which reestablishes a bond that Laine et al. proposes is key to the inter-conversion of KIT between its active and inactive states: the H(hydrogen)-bond between residues Y823 and D792.

We find that EDS did a better job than BFS at capturing key characteristics of KIT’s allosteric communication. We attribute EDS’s better performance to its path construction being more sensitive to shifts in the position of residues. In particular, EDS shows a clear advantage over BFS in the recovery of known mutational hotspots. We hope that the positive results reported here will inspire others to consider local search when studying protein structure networks, and to design new approaches to analyze proteins on a large scale in a high-throughput manner.

2. Method and Materials

2.1 Protein Residue Network (PRN)

A PRN is constructed from the coordinates obtained from PDB (rcsb.org) or the snapshots of a MD run. A PRN is a simple undirected connected graph $G = (V, E)$. Each element in the set of nodes V represents an amino acid molecule (residue) in a protein sequence. Let the number of nodes $|V| = N$. Nodes are labeled by the residue id (*rid*) given in the coordinates file (so that gaps in node labels correspond in size to gaps in sequence locations).

Our PRN construction is based on the method in [15] which highlights the role protein side-chain atoms play in identifying well-formed protein structures as opposed to a pure $C\alpha$ - $C\alpha$ construction where only the protein backbone is taken into account. Two nodes u and v are linked if and only if $|u - v| > 1$,

and their interaction strength I_{uv} is above a threshold. $I_{uv} = \frac{n_{uv} \times 100}{\sqrt{R_u \times R_v}}$ where n_{uv} is the number of distinct

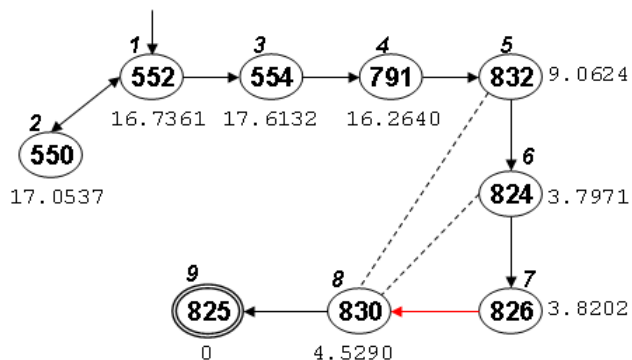
pairs (i, j) such that i is an atom of residue u , j is an atom of residue v , and the Euclidean distance between atoms i and j is within a cutoff distance. R_u and R_v are extracted from a table of normalization values by residue type (Table 1 in [16]). When computing I_{uv} to demonstrate the role side-chains play in specifying protein structure, only side-chain atoms were used in [15]. However, when constructing a classifier to distinguish native from decoy protein folds, hydrogen bonds from the main-chain were included. In contrast to [15], we use both the side-chain and the protein backbone atoms of an amino acid. Our cutoff distance is 7.5 Å and $I_{uv} \geq 5.0$. Values for these parameters were set through trial and error with the goal of creating PRNs that are singly connected without being unnecessarily dense. As in [15], the covalent bonds between amino acids or peptide bonds are ignored. This is appropriate since validation of our model relies heavily on results from ref. [2] where peptide bonds are also ignored.

When necessary to distinguish PRNs by source, let $PRN0$ be the PRN that is constructed from the protein’s PDB file as opposed to a MD snapshot. The set of links E is partitioned into short-range (SE)

and long-range (*LE*) links. A link (u, v) is long-range if and only if $|u - v| > 10$, and short-range otherwise [12].

2.2 The Euclidean Directed Search (EDS) algorithm and shortcut edges

At each step of a search, EDS surveys the proximity to target of the current node’s direct neighbors in a PRN, and moves to a node x not yet on the path and that is closest (Euclidean distance) amongst all nodes surveyed so far to the target node. It is possible that x is not adjacent to the current node. In this case, EDS retraces its steps (*backtrack*) until x becomes reachable. Pseudo-code for the EDS algorithm appears in Appendix A. An edge (u, v) is a *shortcut* if and only if $L^T(v) = L^T(u) + 1$, and v is adjacent to a node w such that $L^T(w) < L^T(u)$. $L^T(x)$ is a positive integer denoting the *order* EDS visits nodes in a path T for the first time. Fig. 1 gives an example of an EDS path with their node visit order labeled. Shortcut edges are marked in red in Fig. 5 (right). The shortcut edges are dominated by short-range links (Fig. 5 left), in accordance to previous observation on other PRNs [8].



PRN edges are undirected, but the edges are oriented in the diagram in the direction they are traversed by EDS in the respective paths. Un-oriented (dashed) edges are not traversed, but exist and play a role in determining whether an edge is a shortcut. Shortcut edges are marked in red. Bidirectional edges are backtrack edges. The real number besides each node is the node’s Euclidean distance to the target node. The italicized integer besides each node x is the node’s first visit order, $L^T(x)$.

Fig. 1 An EDS path that starts in JMR, visits a node (791) in the catalytic-loop and terminates in the A-loop. The EDS path (552, 550, 552, 554, 791, 832, 824, 826, 830, 825) is of length nine.

We ran BFS and EDS for all node pairs (u, v) where $u \neq v$. The number of paths is then $N(N-1)$. Short-range paths (*SP*) are paths connecting source and target node-pairs within (\leq) 10 residues apart on the protein sequence. Paths that are not short-range are long-range paths (*LP*).

2.3 Communication pathways (CP)

A communication pathway (*CP*) is composed of a chain of residues non-covalently bonded (hence the condition $|u - v| > 1$ when constructing a PRN), such that each link in the chain is stable, and the commute time between *any* pair of residues in the chain is small [2]. A link is *stable* if it has high occupancy, i.e. is present in a large fraction (above a threshold e.g. $\geq 50\%$) of the protein’s native ensemble (conformations generated in a MD simulation of the protein’s native dynamics). The *commute time* between a pair of residues (i, j) is the (population) variance of the Euclidean distance between (i, j) in the protein’s native ensemble. A larger variance increases commute time and decreases communication propensity between a residue pair. Euclidean distance is calculated between the carbon-alpha ($C\alpha$) atoms of a residue pair.

There is a major difference between CPs and both EDS and BFS paths. CPs are akin to a constrained diffusion process from a source node (paths or chains linking residues are extended out from a node until there are no more links with acceptable stability and commute time), than to an unconstrained targeted search for a node. Further, there may be no CPs extending out from some residues, but all pairs of nodes are connected by EDS and BFS paths.

However our aim here is not to construct CPs but to evaluate EDS and BFS paths in terms of their stability and communication propensity. Thus we need a way to quantify stability and commute time for a path. Let $sb(e)$ be stability of a link e , i.e. fraction of time it is present in a sequence of MD snapshots. Assuming links of a PRN are independent of each other (this is not entirely true because of geometric

constraints), stability of a path p with n edges is $sb(p) = \prod_{i=1}^n sb(e_i)$. Paths with larger $sb(p)$ are more stable.

Path commute time is the average commute time between *all* pairs of nodes on the path. A path of length λ has $\lambda(\lambda+1)/2$ node pairs; some of the node pairs on an EDS path with backtrack may not be distinct from each other, and commute time between a node and itself is zero. When MD simulation data is not available, we use *estimated path commute time*, which for a path p is the average Euclidean distance between *all* pairs of nodes on p . Estimated path commute time is based on the Euclidean distance of residue pairs in a static protein structure, whereas path commute time is based on the commute time of residue pairs calculated from an MD simulation.

2.4 Independent dynamic segments (IDS)

An independent dynamic segment is a cluster of residues whose atomic fluctuations are correlated with each other, but whose dynamical behavior is independent from other IDSs [2]. Residues of the 10 IDS for the wild type (WT) KIT are extracted from Table S1 of [2] and reproduced in Table 1. The WT IDSs are marked on the 1T45 molecule in Fig 2 (left). There is a loop component to all the IDSs which gives them the flexibility to have their own independent dynamics. WT IDS residues involve 18.87% of its 159 alpha-residues, 12.73% of its 55 beta-residues and 54.70% of its 117 loop-residues.

Table 1 List of residues in each WT IDS and the region of interest in which each IDS is situated [2]. # is number of residues in an IDS.

Region	IDS	WT	#
JMR (547...581)	S1	547...554	8
	S2	561...569	9
	S3	574...581	8
	S4	588, 609...618	11
	S5	626...633	8
	S6	585...587, 661...666	9
	S7	688...694, 753...762	17
A-loop (810...835)	S8	824...831	8
	S9	870...882	13
	S10	926...935	10
Total number of IDS residues			101

2.5 Hub residues

Hub residues are residues that lay on many communication pathways [2]. These hub residues are either evolutionarily conserved or have been observed to participate in the regulation of other receptor tyrosine kinases and cytoplasmic kinases. The 71 hub residues identified in [2] for WT are: 649...655 (C-loop-2), 764...785 (E-helix), 790...797 (catalytic-loop), 804...808 (β -strand B8), 835...843 (P+1 loop), 850...865 (F-helix), and 678, 798, 799, 800, 858, and 862 (catalytic spine). These residues are marked in red in Fig. 3 (left).

2.6 Mutational hotspots

Apart from D816, several other point mutations have been documented to trigger irregular state change in KIT. These mutational hotspots include V560, V654, T670, D820, N822 and A829 [2]. The yellow colored sticks in Fig. 3 (right) mark the positions of these seven mutational hotspot residues.

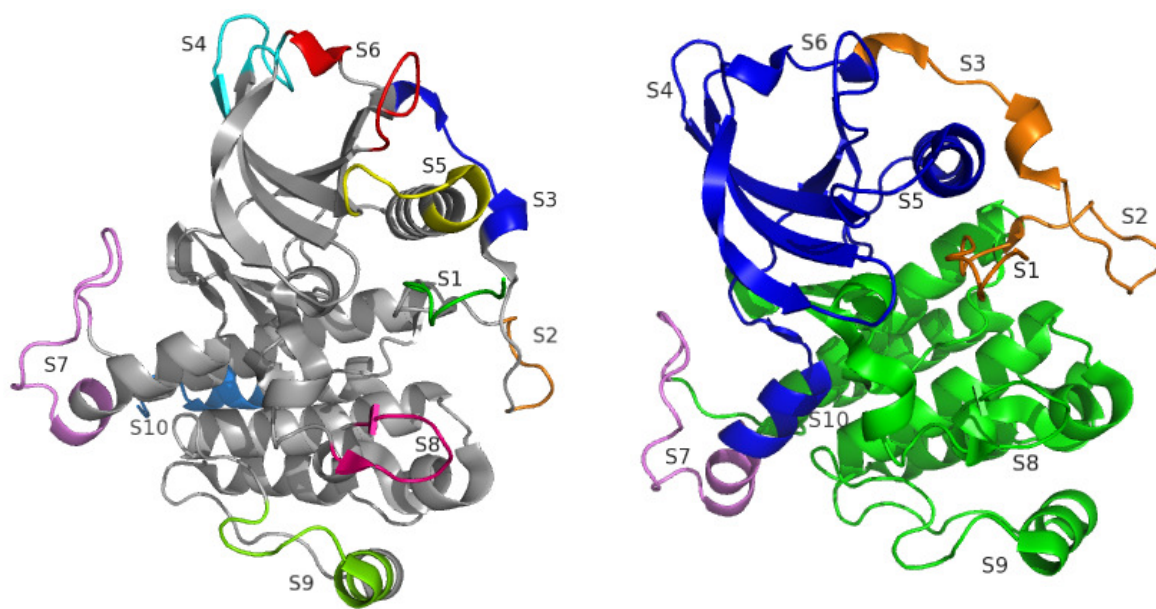


Fig. 2 Left: The ten WT IDs in Table 1 are colored differently on the cartoon of 1T45 and labeled accordingly. S1, S2 and S3 are in the JMR, and S8 is in the A-loop region. Right: A cartoon of 1T45 with the JMR colored orange, the N-lobe (582...684) blue, the C-lobe (762...935) green, and the pseudo-KID (685...694, 753...761) violet. S4, S5 and S6 are located in the N-lobe, while S8, S9 and S10 are in the C-lobe.

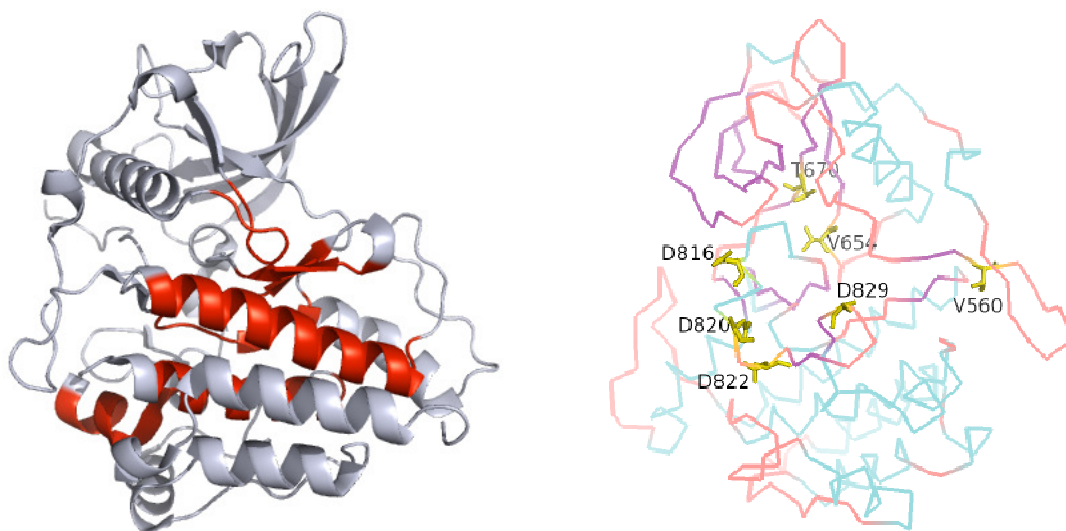


Fig. 3 Left: The 71 hub residues identified in [2] are in red on a cartoon of 1T45. Right: The seven mutational hotspots referenced in [2] are shown as yellow sticks on a ribbon representation of 1T45.

2.7 The 1T45 (WT) PRN

The 1T45 PRN has 331 nodes and 2314 edges, of which 573 are shortcut edges. Three very stable H-bonds were identified in [2] as playing a key role in the communication between the JMR and A-loop regions of inactive KIT: Y823-D79, D792-H790, and H790-N797. The occupancy rates for these three H-bonds in the MD simulations of WT were 95%, 95%, and 93% respectively [2]. These three residue pairs are linked in the 1T45 PRN, and their $C\alpha$ to $C\alpha$ Euclidean distances are 10.31720, 5.57263 and 9.79231 respectively (units in Angstrom \AA).

Using a large distance cut-off value can be problematic for pure Ca-Ca *residue interaction networks* (RINs) as structural variations may be smeared away. A pair of amino acids (nodes) in a RIN is connected by an edge if the Euclidean distance between their Ca atoms is within a certain user specified threshold range. Our method of PRN construction is less susceptible to this problem as PRNs are weaker expander graphs (and therefore more modular) than RINs [8]. Fig. 4 illustrates this point on the 1T45 PRN and two RINs: one with 10.3172 Å as the distance cutoff, and another with 15.5677 Å. The RINs have many more edges that cross large cavities on the molecular surface.

In the 1T45 PRN, edges between residues of the same (WT) IDS are short-range (SE) (left triangle of Fig. 5-left). Compared to the connectivity of all 1T45 PRN nodes, WT IDS nodes have significantly smaller degree (9.74 on average), and a significantly larger fraction of their links (67% on average) are SE (Table 2). Compared to all 1T45 PRN nodes, the hub residues (section 2.5) have significantly larger node degree (18.01 on average), and a significantly larger fraction of their links (56% on average) are long-range (LE) (Table 2).

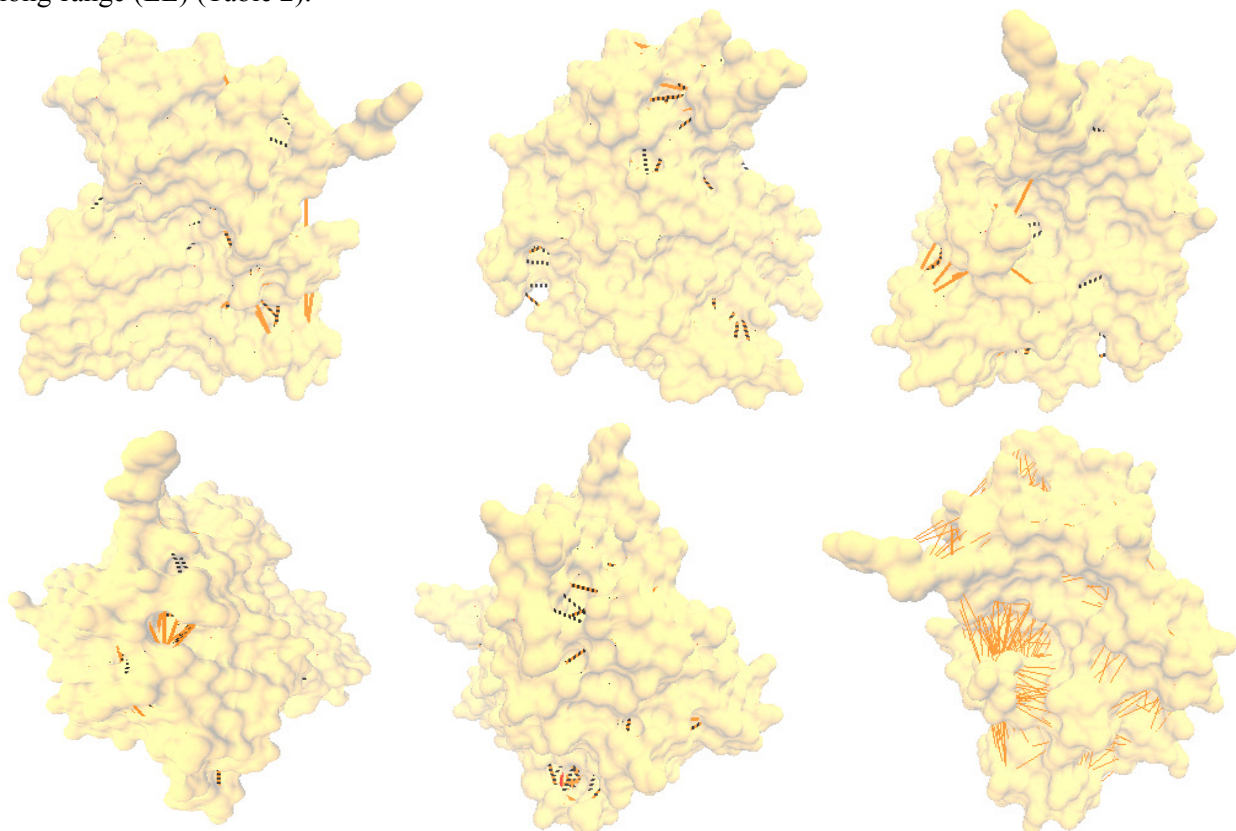


Fig. 4 Six views of 1T45 showing cavity crossings by PRN and RIN edges. The surface of the 1T45 molecule was drawn with VMD [17] SURF at a probe radius of 1.4 Å. The dotted lines in black are non-shortcut PRN edges. The orange solid lines are RIN edges. The 1T45 RIN edges in the first five panels have a maximum Euclidean distance (measured Ca to Ca) of 10.3172 Å (just long enough for 792-823 to be an edge). This RIN has 2906 edges. The 1T45 PRN edges have a maximum Euclidean distance (measured Ca to Ca) of 15.5677 Å. Due to their short-range propensity (Fig. 5 left), PRN shortcut edges that cross cavities are rare. The bottom centre panel shows an instance of cavity crossing by a PRN shortcut edge (shown as a red solid line in a cavity at the bottom). The 1T45 PRN shortcut edges have a maximum Euclidean distance (measured Ca to Ca) of 10.6672 Å. The bottom right panel is a view of 1T45 with RIN edges at a cutoff of 15.5677 Å. This RIN is more dense; it has 9139 edges and show many more cavity crossing edges.

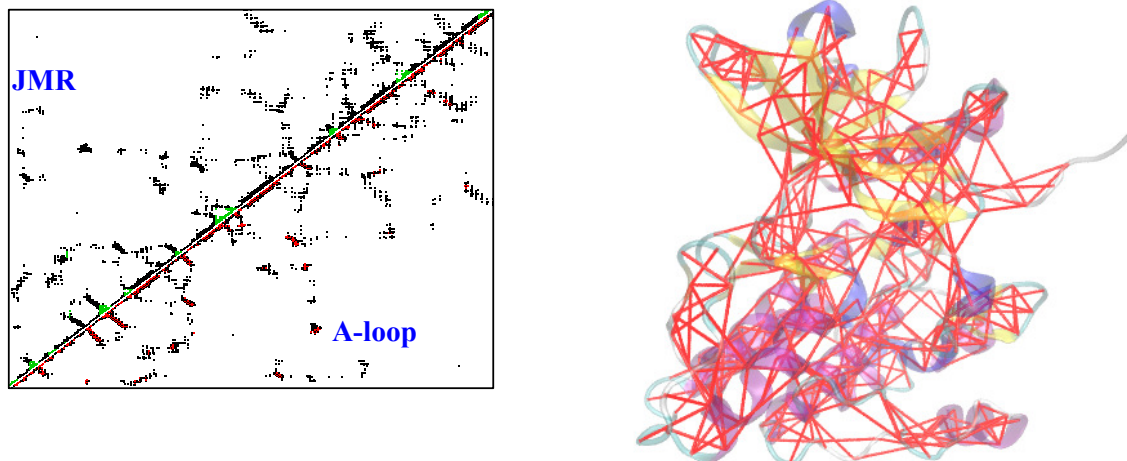


Fig. 5 Left: Adjacency matrix (contact map) of the 1T45 PRN; the A-loop is to the right of the JMR. Intra-IDS edges are marked in green, shortcut edges are marked in red, and all other edges are in black. Both intra-IDS edges and shortcut edges are dominated by short-range links as they are primarily located near the main diagonal. Right: Shortcut edges are drawn in red on a cartoon of the 1T45 molecule.

Table 2 Connectivity (mean \pm std. dev.) of nodes in the 1T45 PRN. Hubs are most connected, while IDS nodes are least. Compared to all nodes, a significantly larger proportion of links incident on IDS nodes are short-range (SE), while a significantly larger proportion of links incident on hub nodes are long-range (LE).

	Node degree	Fraction of node links that are SE	Fraction of node links that are LE
All nodes	13.9800 \pm 5.2766	0.5191 \pm 0.2214	0.4809 \pm 0.2214
IDS nodes	9.7430 \pm 4.1028	0.6709 \pm 0.2229	0.3291 \pm 0.2229
Hub nodes	18.0100 \pm 4.3408	0.4350 \pm 0.1490	0.5650 \pm 0.1490

Significance of differences is determined with one-sided Wilcoxon test.

The largest p-value over all tests is 0.001964. $a > b$ means a is significantly larger than b .

Degree	Hub > All > IDS
SE fraction	IDS > All > Hub
LE fraction	Hub > All > IDS

3. Results and Discussion

3.1 Path stability and path commute time

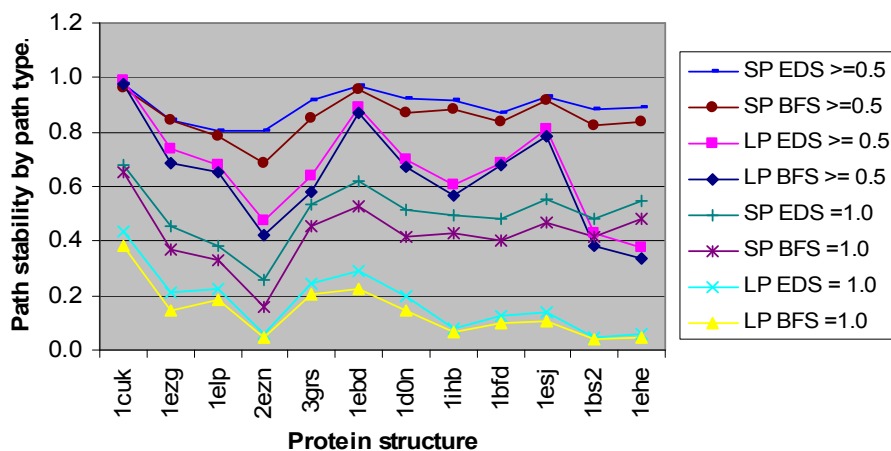
We evaluated path stability and path commute time of EDS and BFS paths on PRNs of 12 randomly selected proteins (Table 4) whose native dynamics (298K) is available in the Dymameomics database [18, 19]. A *PRN0* was constructed for the chain of each protein within the residue range simulated in Dymameomics. Except for 2EZN (Model 1) where the entire MD simulation was used, stability and commute times of links were computed using the first x of the y available MD native dynamics snapshots. (This is due to data download constraints. We experimented with fewer snapshots for 2EZN and could arrive at the same general conclusion; nonetheless using the whole native ensemble is preferable.) With these link stability and link commute time information, path stability and path commute time were calculated for the set of all EDS and BFS paths of each protein's *PRN0*. We are mainly interested in long-range paths (LP) with more than one edge.

Over all paths of length greater than one, EDS paths are significantly more stable and have significantly smaller commute times (better communication propensity) than BFS paths. This conclusion also holds when the analysis is broken down by path type (Fig. 6 & Table 4). Both short- and long-range EDS paths are significantly more stable and have significantly better communication propensity than BFS paths of the same type. The short-range paths of both BFS and EDS exhibit significantly better stability

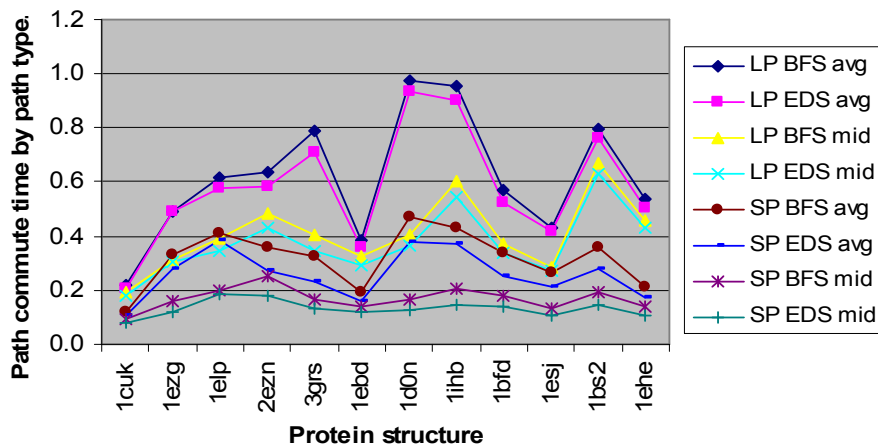
and significantly higher communication propensity than their respective long-range paths. These findings support the notion that EDS paths are more plausible intra-protein communication pathways than BFS paths.

Table 3 PDB code and basic statistics for the 12 proteins.

PDB code (residue range used)	MD snapshots used/total	Number of PRN0 nodes	Number of PRN0 links		Number of paths with > 1 edge in PRN0	
			Short-range (SE)	Long-range (LE)	Short-range (SP)	Long-range (LP)
1CUK-A (156-203)	20,000/51,163	48	178	65	494	1,276
1EZG-A (2-83)	20,000/52,490	82	326	324	878	4,464
1ELP-A (1-83)	20,000/52,318	83	215	328	1,120	4,600
2EZN-A (1-101)	51,000/51,000	101	346	491	1,218	7,208
3GRS-A (366-478)	20,000/53,650	113	330	329	1,490	9,848
1EBD-A (155-271)	20,000/53,224	117	335	354	1,560	10,634
1D0N-A (27-159)	20,000/51,311	133	386	431	1,778	14,144
1IHB-A (5-160)	20,000/51,867	156	587	489	1,836	20,192
1BFD-A (2-181)	20,000/52,997	180	561	712	2,368	27,306
1ESJ-A (1-272)	20,000/52,274	272	939	1,065	3,452	66,252
1BS2-A (136-482)	12,000/51,989	347	1,208	1,164	4,414	110,904
1EHE-A (5-404)	12,000/51,560	399	1,430	1,391	5,010	148,150



SP EDS ≥ 0.5 denotes the fraction of EDS short-range paths with > 1 edge with path stability of at least 0.5.
LP BFS = 1.0 denotes the fraction of BFS long-range paths with > 1 edge with path stability of 1.0.



LP BFS avg denotes the average path commute time of long-range BFS paths.
SP EDS mid denotes the median path commute time of short-range EDS paths.

Fig. 6 Top: Short-range paths are more stable than long-range paths. EDS paths are more stable than BFS paths. **Bottom:** Long-range paths have longer commute times than short-range paths. BFS paths have longer commute time than EDS paths.

This result follows from the link usage pattern observed in [8], coupled with the differences in stability and commute times of links of different types. Compared with BFS paths, EDS paths have a significantly weaker propensity to use long-range links (LE) than short-range links (SE) [8], and SE are significantly more stable and have smaller commute time than LE (Table 4). A pair of residues with small commute time means the Euclidean distance between their pair of *Ca* atoms has not varied much over time (the MD native dynamics snapshots). It stands to reason that if a link exists between such a pair, the link is expected to be highly stable. Table 4 also shows that shortcut edges (*SC*), which are enriched with short-ranged links [8], are significantly more stable and have smaller commute time than non-shortcut edges (*NSC*). *SC*s are more central than *NSC*s; they are traversed by significantly more EDS paths on average than *NSC*s [8].

Table 4 p-values generated with R’s Wilcoxon one-sided test, paired when possible (path comparisons). For all the 12 PRN0s, *LP* EDS paths are significantly (p-value < 0.05) more stable than *LP* BFS paths, and *LP* EDS paths have significantly smaller path commute time than *LP* BFS paths. Except for 1EZG, short-range links (*SE*) in PRN0s are significantly more stable and have significantly smaller commute time than long-range links (*LE*) in PRN0s. Except for 1EZG, shortcut links (*SC*) are significantly more stable and have significantly smaller commute time than non shortcut links (*NSC*).

PRN0	<i>LP</i> path stability	<i>LP</i> path commute time	Edge stability		Edge commute time	
	BFS < EDS	BFS > EDS	<i>SE</i> > <i>LE</i>	<i>SC</i> > <i>NSC</i>	<i>SE</i> < <i>LE</i>	<i>SC</i> < <i>NSC</i>
1CUK-A	2.07E-02	5.20E-19	2.68E-09	2.05E-03	1.32E-25	2.66E-07
1EZG-A	9.02E-29	1.45E-02	3.68E-01	1.82E-09	2.57E-07	1.92E-01
1ELP-A	2.13E-09	4.21E-25	1.83E-03	2.77E-10	1.39E-09	1.98E-05
2EZN-A	9.45E-23	2.53E-82	8.40E-31	1.54E-42	1.80E-52	1.19E-27
3GRS-A	4.42E-51	1.90E-106	4.94E-14	6.15E-14	1.87E-24	1.10E-14
1EBD-A	5.35E-60	3.57E-115	3.31E-10	7.49E-11	9.06E-31	1.74E-15
1D0N-A	5.25E-46	7.34E-86	3.05E-19	1.99E-19	9.84E-29	7.12E-23
1IHB-A	1.18E-59	2.11E-140	1.46E-73	6.89E-21	2.40E-103	2.28E-24
1BFD-A	1.30E-25	4.61E-236	2.68E-43	3.89E-24	5.09E-63	3.24E-26
1ESJ-A	1.57E-165	2.22E-267	8.06E-67	2.43E-30	9.46E-147	7.79E-43
1BS2-A	2.33E-281	0.00E+00	1.01E-113	2.07E-54	5.28E-187	1.54E-67
1EHE-A	0.00E+00	0.00E+00	4.92E-143	7.89E-65	8.34E-247	2.57E-76

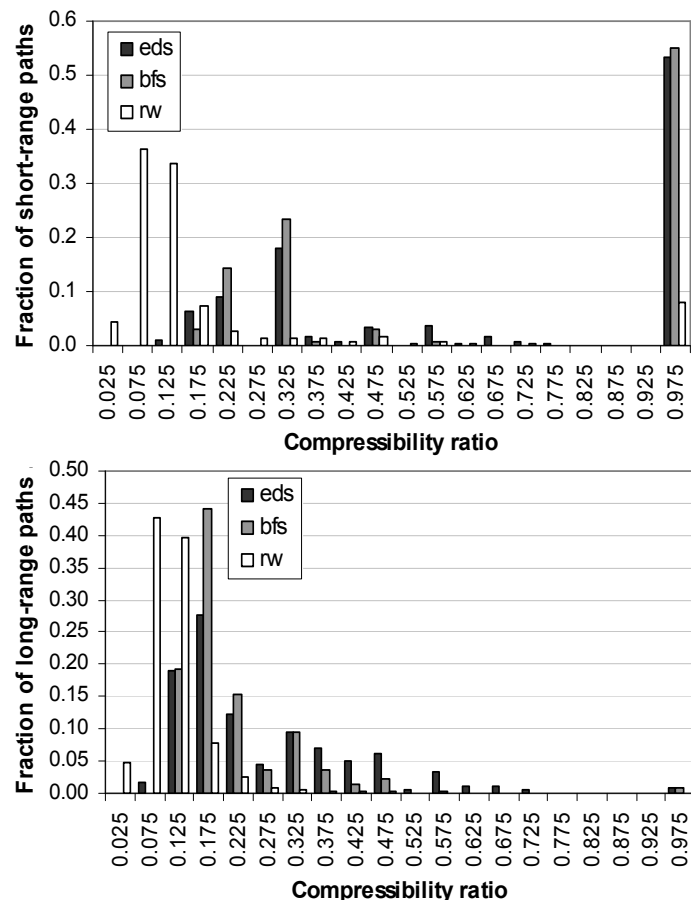
3.2 Compressibility of paths

As a preliminary investigation to assess the feasibility of using EDS or BFS paths to detect IDSs, we analyze the compressibility of three types of paths on the WT PRN: EDS, BFS and paths generated by a random walk (*RW*). A *RW* moves to a direct neighbor node of the current node, selected uniformly at random, until the target node is found. Random walks on a network that has modular structure spend more time wandering amongst nodes of a module than traversing between modules. This is the common principle exploited by flow-based clustering algorithms [20, 21]. It is expected then that if each module in a network were labeled uniquely but nodes of the same module were labeled identically, and a path *p* is a sequence of node labels in the order the nodes are visited by *p*, paths which follow the modular contours of a network more faithfully would be more *compressible*. A path represented as a string of symbols is compressible if it has a sub-string of length greater than one that is comprised of identical symbols. Let $\text{nodes}(p)$ be the number of nodes in path *p*. The *compression ratio* for a path is $cr(p) = [\text{nodes}(p) - \text{nodes}(cp)] / \text{nodes}(p)$ when $\text{nodes}(cp) > 1$ and $cr(p) = 1$ when $\text{nodes}(cp) = 1$. Larger *cr* values imply greater compression. $cr = 0$ when there is no compression, and a path with maximum compression ($cr = 1$) stays within a single module.

To compute *cr* for all paths on the WT PRN, we first assigned each of the 10 WT IDS with a unique identifier such that the set of IDS identifiers are distinct from the set of node labels of the WT PRN. We then replaced the node labels with their respective IDS identifiers when possible, and analyzed the *cr* values by path range. The WT PRN has 1151 short-range paths (*SP*) and 15999 long-range paths (*LP*).

The distribution of cr values is not normal and highly skewed (Fig. 7). The RW paths are significantly more compressible than both the EDS and BFS paths, and this difference holds when paths are examined by range. The EDS paths are significantly more compressible than the BFS paths, and this result holds when SPs and LPs are examined separately. We conclude that EDS paths follow the modular contours of the WT PRN more so than BFS paths.

For both EDS and BFS paths, SPs are significantly more compressible than LPs. The distribution of SP cr values for both EDS and BFS skew to the left (many more short-range paths have large cr), while the distribution of LP cr values skew to the right (many more long-range paths have small cr). In contrast, the distribution of SP and LP cr values for RW both skew to the right, and RW LP are significantly more compressible than RW SP (Fig. 7).



Number of paths by type	Mean and std. dev. cr		
	RW	EDS	BFS
Both	0.1025	0.0721	0.0501
109230	± 0.0643	± 0.1569	± 0.1246
Short	0.1151	0.1546	0.1357
1151	± 0.1369	± 0.3213	± 0.3084
Long	0.1017	0.0670	0.0448
15999	± 0.0567	± 0.1387	± 0.1004

$a > b$ means $cr a$ is significantly larger than $cr b$. Significance of differences is determined with one-sided Wilcoxon test, paired when possible. The largest p-value over all tests is $1.204e-08$.

	eds	bfs	seds	sbfs	lrw	leds	lbfs
rw	>	>					
eds		>					
srw			>	>	<		
seds				>	<	>	
sbfs					<		>
lrw						>	>
leds							>

Naming convention:
 rw = random walk
 s prefix = short-range paths
 l prefix = long-range paths

Fig. 7 Distribution and comparison of compression ratios cr

3.3 Locating independent dynamic segments (IDS)

The task is to produce clusters that match the WT IDSs as closely as possible. Ideally, all members of a generated cluster would belong to the same IDS, and all members of an IDS would be found within the same generated cluster. The clusters are generated with MCL [21], which is a freely available (micans.org/mcl) flow-based clustering algorithm that has found application in bioinformatics, e.g. [22, 23]. Our input to MCL is in ABC-format which means a triple (u, v, w) per line where u and v is a node pair and w is the strength of their similarity. MCL works better with undirected relationships, and so in cases where there is a directed relationship, e.g. edge usage depends on direction the edge is traversed, we tested with the sum and the maximum of the scores in both directions. We experimented with 24 similarity scores (Table 5). The main MCL tuning parameter is I (inflation), which influences the number of clusters produced. We set I at 1.4, 1.6, 1.8, 2.0 and 2.2 for each similarity score tested.

Each set of clusters produced by MCL is evaluated with the methodology in [23] which uses the notion of Accuracy and Separation. Better cluster prediction is associated with larger values for both Accuracy and Separation, and the maximum is 1.0 for both. $Accuracy = \sqrt{Sn \times PPV}$, and it measures how well the IDSs are covered by their respective best-matching cluster, and conversely how well the clusters overlap their respective best-matching IDS. Let Z be the total number of residues or nodes over all IDSs, n be the number of IDSs, m be the number of MCL clusters that overlap at least one IDS, and T be a $n \times m$ table where entry T_{ij} is the number of nodes in IDS i and MCL cluster j . $Sn = \frac{1}{Z} \sum_{i=1}^n \max(T_i)$, where $\max(T_i)$ is the maximum entry in row i of T . $PPV = \frac{1}{Z} \sum_{j=1}^m \max(T_j)$, where $\max(T_j)$ is the maximum entry in column j of T . Having multiple IDSs in one cluster lowers PPV , and having an IDS spread out over multiple clusters lowers Sn . $Separation = \sqrt{\frac{J^2}{n \times m}}$, and it measures the cohesiveness of the IDSs and MCL clusters. While $Accuracy$ is concerned only with the size of the largest overlap for each IDS and each cluster, $Separation$ takes into account the number of cluster fragments per IDS, and conversely the number of IDS slices per cluster. For instance, an IDS of size 8 could fragment in different ways over three clusters as: 1, 5, 1; 4, 2, 2 or 3, 1, 4. The first configuration is most cohesive. J builds on the idea of the Jaccard similarity index. $J = \sum_{i=1}^n \sum_{j=1}^m \frac{(T_{ij})^2}{sum(T_i) \times sum(T_j)}$, where $sum(T_i)$ is the sum of the entries in row i of T (or the number of residues in IDS i), and $sum(T_j)$ is the sum of the entries in column j of T (or the number of residues in cluster j that belong to some IDS). $\sum_{i=1}^n sum(T_i) = \sum_{j=1}^m sum(T_j) = Z$.

Table 5 Similarity scores used as input to the MCL clustering algorithm.

Name	Description
<i>edge</i>	All PRN edges (u, v) with equal weight of 1.
<i>wedge</i>	All PRN edges weighted with 1 for non-shortcut edge and with 2 for shortcut edge.
<i>sele</i>	All PRN edges weighted with 1 for long-range edge and with 2 for short-range edge.
<i>scut</i>	All shortcut edges only, with equal weight of 1.
<i>euc_dist</i>	All PRN edges weighted by the Euclidean distance between an edge's endpoints.
<i>interact</i>	All node pairs with interaction strength $I_{uv} > 0$.
<i>X_max</i>	PRN edges weighted by maximum usage of an edge by X , i.e. weight of (u, v) is the maximum of X 's usage of (u, v) and X 's usage of (v, u) . X is either RW, EDS or BFS, and all three options are used.
<i>X_sum</i>	PRN edges weighted by total usage of an edge by X , i.e. weight of (u, v) is the sum of X 's usage of (u, v) and X 's usage of (v, u) . X is either RW, EDS or BFS, and all three options are used.
<i>sX_max</i>	Same as <i>X_max</i> except only short-range paths are considered.
<i>sX_sum</i>	Same as <i>X_sum</i> except only short-range paths are considered.
<i>lX_max</i>	Same as <i>X_max</i> except only long-range paths are considered.
<i>lX_sum</i>	Same as <i>X_sum</i> except only long-range paths are considered.

The cluster evaluation results are reported in Fig. 8 where comparisons are made with the best result (maximum Accuracy \times Separation) for a similarity score. The best two outcomes are yielded by *seds_max* and *sbfs_max*, both with I at 1.6. *seds_max* with $I = 1.6$, yielded the maximum Accuracy \times Separation score of 0.8247. In general, clusters generated with RW similarity scores outperform the clusters produced with EDS similarity scores, and the EDS clusters in turn outperform the BFS clusters. Except for RW, clusters generated using only short-range paths (*seds_* and *sbfs_*) outperform clusters generated using only long-range or all paths. These clustering results concur with the significant differences in *cr*

values reported in Fig. 7, and there is a strong and positive correlation (0.8830) between cr values and the best results for clusters produced with path information.

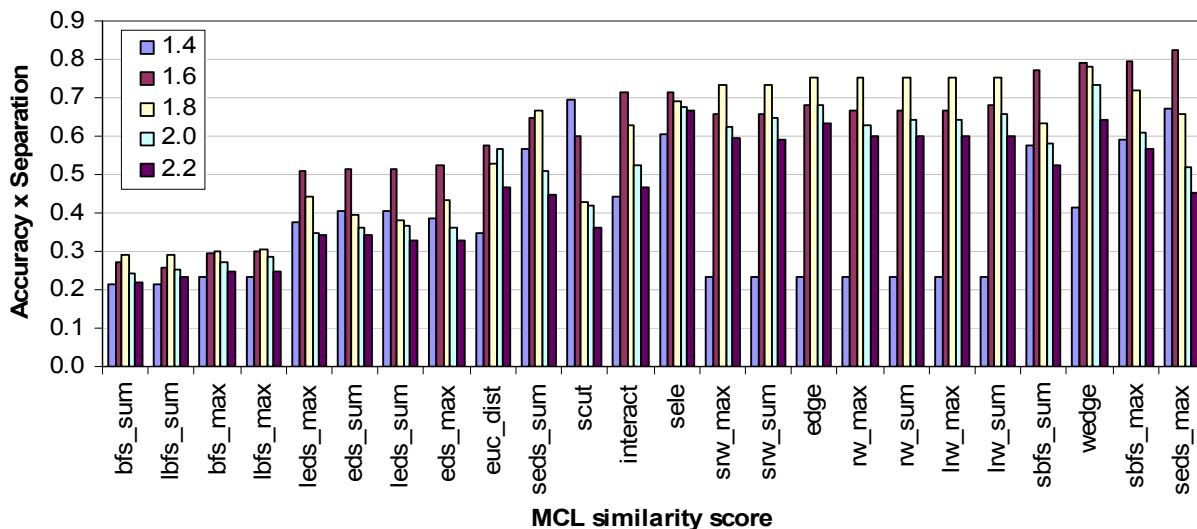


Fig. 8 Evaluation of MCL clusters against the reference set of WT IDSs. The best MCL similarity score, *seds_max* with $I = 1.6$, yields an Accuracy x Separation score of 0.8247.

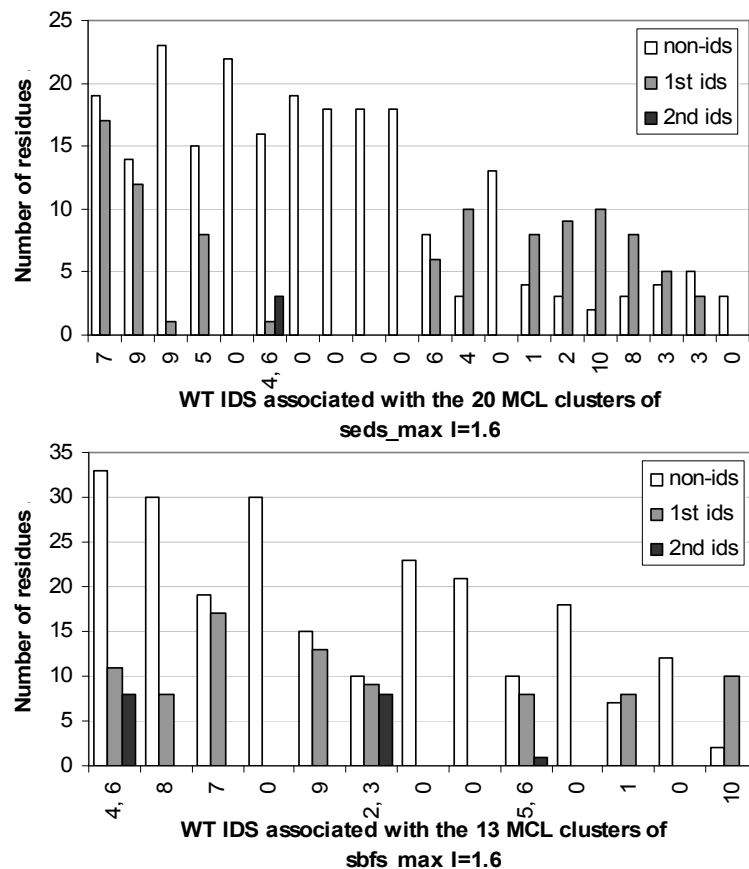


Fig. 9 Mapping of the two best MCL clusters to the 10 WT IDSs. For each MCL cluster, the bar chart plots the number of residues that do not belong to any IDS (non-ids), and the number of residues for each IDS that overlaps the cluster. The x-axis is labeled with the IDSs found in a cluster. Several MCL clusters are not associated with any IDS. This is expected since IDS residues cover only about a third (101/331) of the WT PRN nodes.

Fig. 9 takes a closer look at these two best sets of MCL clusters. *sefs_max* ($I=1.6$) has only one cluster with more than one IDS but four IDSs (S3, S4, S6 and S9) that overlap more than one cluster each. In contrast, *sbfs_max* ($I=1.6$) has three clusters with more than one IDS, and only one IDS (S6) spread over more than one cluster. *sbfs_max* ($I=1.6$) is ranked lower than *sefs_max* ($I=1.6$) mainly because it has a smaller *Accuracy* value due mainly to S2 and S3, which are about the same size, occupying the same cluster. The third best outcome was produced by *wedge* with I also at 1.6. The *wedge* similarity score weights shortcut edges at 2 and non-shortcut edges at 1. The *sele* similarity score weights short-range edges at 2 and long-range edges at 1 (Table 5). Shortcut edges are predominantly short-range links [8] (Fig. 5-left). That *wedge* outperforms *sele* supports the notion that shortcut edges identified by the EDS algorithm are a distinct and pertinent subset of PRN edges.

3.4 Communication between WT IDSs

IDSs correspond to well known functional regions distributed throughout KIT [2]. In particular, IDSs S1, S2 and S3 reside within the JMR (547...581) and IDS S8 resides within the A-loop region (810...835). In the inactive form, these two regions interact allosterically. Our task here is to examine how well these two regions are connected by EDS and BFS paths.

We do this by first constructing a weighted complete graph comprised of all pairs of IDSs. A pair of IDSs is linked in this graph if a path runs through them. A path may connect one or more IDS pairs, or none at all. It is easier to work with the compressed paths described previously (section 3.2). A compressed path cp connects an IDS pair (y, x) if both x and y appear in cp . The weight of the link between x and y is the number of such cp compressed paths, normalized so that weights of a graph sum to 1.0. The weight of a link in an IDS interaction network quantifies the communication strength between an IDS node pair, with heavier weights indicating stronger communication. Note that only 5/45 of the IDS pairs are directly connected to each other by a link between their residues, and there are only 32 such links.

Fig. 10 (top) shows the weights for all links in the three inter-IDS communication networks. Weights in the RW network is fairly uniform, as expected from an unbiased random walk. However, both the EDS and the BFS networks show some strong biases, with heavier weights for links between IDS-pairs S1-S5, S1-S6, S4-S6, S5-S6, and S8-S9. The more intense communication between the last three IDS pairs may be reflecting their co-location within the same lobe, i.e. S4, S5, and S6 are located within the N-lobe, while IDSs S8 and S9 reside in the C-lobe (Fig. 2 right). But more to the point of this section, the weight assigned to IDS-pair 1-8 by EDS is 2.6 times stronger than that assigned by BFS (whose weight is almost the same as RW's), and no other IDS-pair displays such a large weight difference (Fig. 10-bottom). From this, we conclude that the JMR and A-loop regions of inactive KIT are better connected by EDS paths than BFS paths.

3.5 Communication between JMR and A-loop

Allosteric communication between the JMR and A-loop via the catalytic-loop plays an important role in maintaining the stability of inactive KIT [2]. At least one CP originating from the A-loop of WT reached the JMR via the catalytic-loop. We call a path that traverses such a route a *JCA* or *ACJ* path. JCA paths are EDS or BFS paths that visit the JMR, catalytic-loop and A-loop regions exclusively and in order. ACJ paths are EDS or BFS paths that visit the JMR, catalytic-loop and A-loop regions exclusively and in reverse order. Let j_x be a residue in the JMR, c_x be a catalytic-loop residue, a_x be a residue in the A-loop region and $1 \leq p < q < k$, then a JCA path has the form $\langle j_1, \dots, j_p, c_{p+1}, \dots, c_q, a_{q+1}, \dots, a_k \rangle$ while a ACJ path takes the form $\langle a_1, \dots, a_p, c_{p+1}, \dots, c_q, j_{q+1}, \dots, j_k \rangle$.

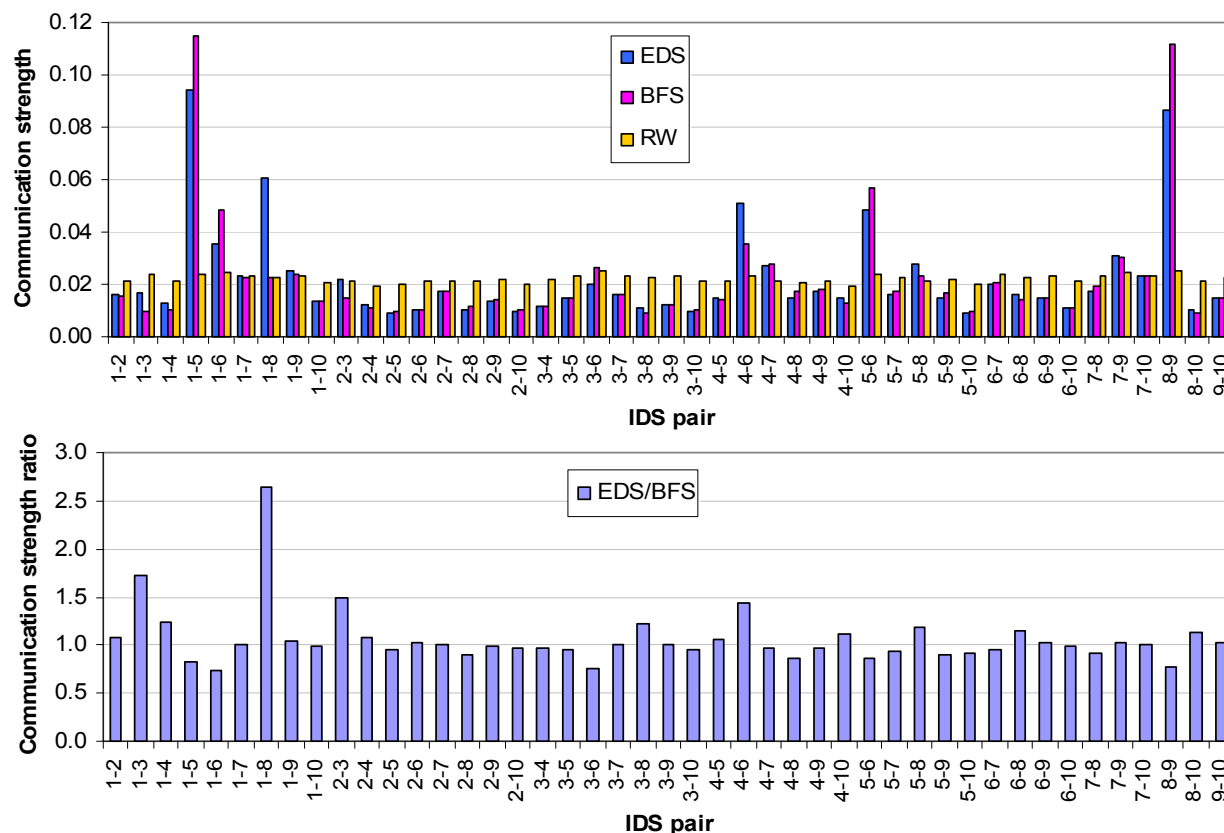


Fig. 10 Inter-IDS communication profile for WT (inactive) KIT. Top: Link weights by IDS-pair for the three IDS interaction network. Bottom: Ratio of EDS to BFS link weights by IDS-pair. A larger weight value is indicative of stronger communication.

EDS made many more JCA or ACJ paths than BFS and although the EDS JCA or ACJ paths were on average significantly longer than the BFS JCA or ACJ paths in terms of graph distance (number of edges in a path), the EDS JCA or ACJ paths have better communication propensity (significantly smaller estimated path commute times) than the BFS JCA or ACJ paths (Table 6). Hence, communication between JMR and A-loop via the catalytic-loop in WT is stronger with EDS than with BFS paths..

Table 6 Statistics for JCA or ACJ paths in the WT PRN

	EDS	BFS
Number of paths	210	150
Path length (mean \pm std. dev.)	4.79 \pm 1.90	3.46 \pm 0.88
Estimated path commute time (mean \pm std. dev.)	13.30 \pm 1.97	13.93 \pm 2.10

3.6 Identifying hub residues

The task is to identify the 71 hub residues (section 2.5) using information generated by EDS and BFS on the 1T45 PRN. A number of complex network approaches have been proposed to identify key residues (for different purposes) in a network of interacting protein residues. These approaches typically employ some notion of network centrality either by degree, number of paths (betweenness) or graph distance (closeness) [5, 6]. We tried several of these centrality measures and found closeness based on estimated path commute time (section 2.3) gave the best outcome. Hub residues display fast commute times [2]. Hence it is reasonable, by definition of commute time, that closeness based on Euclidean distance works best to identify the hub residues.

Closeness for a node x is the total estimated path commute time from x to all other nodes in the network. Nodes with small closeness values are on average nearer to all other nodes in the network than nodes with large closeness values. Closeness was computed with both EDS and BFS paths. For both measures, residues located in the same lobe were closer to each other. N-lobe residues are significantly closer to other N-lobe residues than to C-lobe residues, and C-lobe residues are significantly closer to other C-lobe residues than to N-lobe residues (Fig. 11).

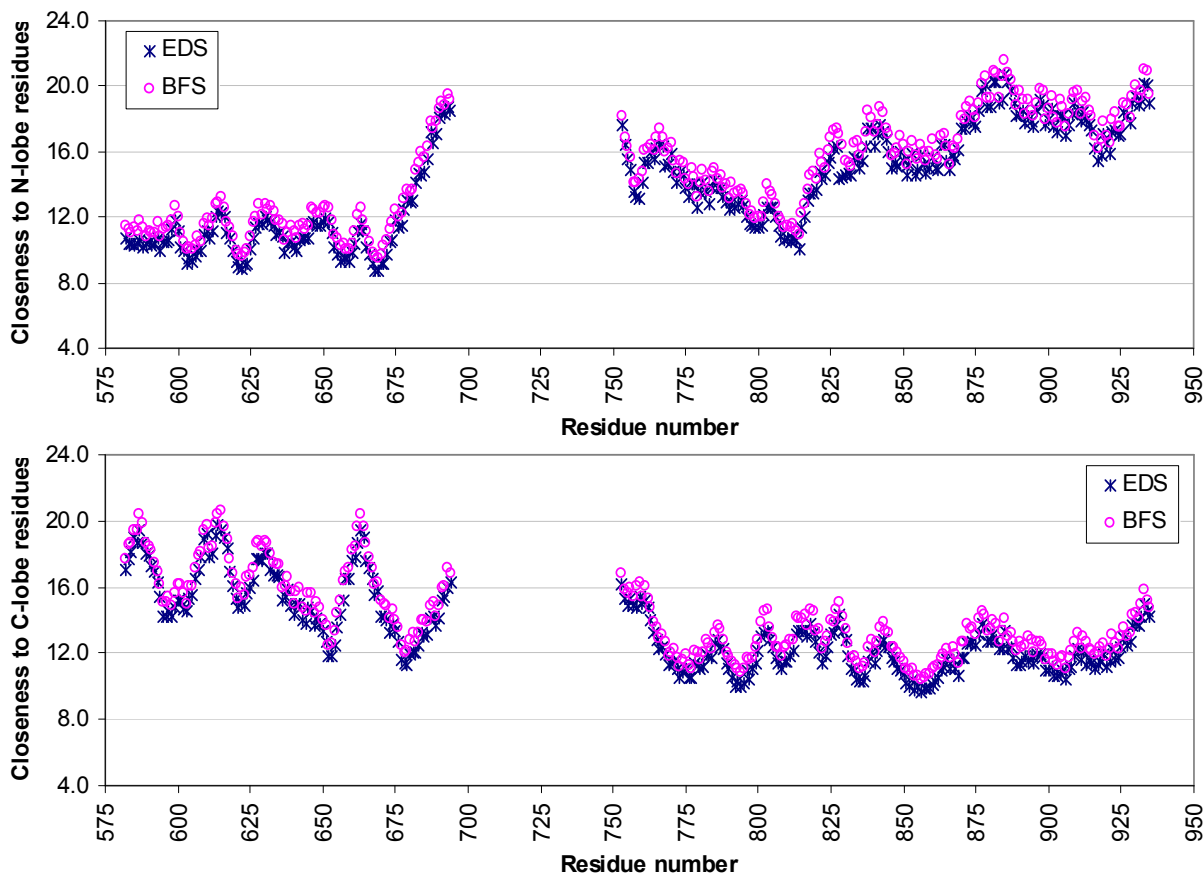


Fig. 11 WT residues in the same lobe are closer to each other than to residues in the other lobe. The gap in the middle (residues 695...752) covers the KID (Kinase Insert Domain), which is excluded for crystallization [14].

To recover the hub residues, the nodes were sorted in non-decreasing order of their closeness values (to both lobes). Nodes with smaller closeness values are enriched with hub residues. It is possible to recover at least 60% of the 71 hubs residues at the cost of 26 false positives (10% of 260) with both EDS and BFS closeness values (Fig. 12). Full recovery is slightly quicker with EDS closeness (61.15% FPR) than with BFS closeness (66.92%). The catalytic-loop plays an important role in channeling communication between the JMR and A-loop regions [2]. The eight hub residues in the catalytic-loop (790...797) were the easiest to recover. They are amongst the top 13 residues with the smallest EDS closeness value, and are amongst the top 18 with the smallest BFS closeness value.

Closeness based on EDS paths performed as well as closeness based on BFS paths (Fig. 12). This result is not unexpected as a strong positive correlation between EDS and BFS betweenness centrality was reported in [8]. Both EDS and BFS closeness outperformed RW closeness convincingly (Fig. 12). Using closeness based only on short-range paths to recover hub residues is not a good strategy as evidenced by the poor performance of both *eds_sp* and *bfs_sp* in Fig. 12. This is expected since hub residues lay on the intersection of many communication pathways, and CPs serve as channels for long-range communication. In contrast, IDS residues originate few or no CPs at all [2]. Compared with all

nodes, WT IDS residues have significantly larger closeness values, while hub residues have significantly smaller closeness values (Fig. 12 right).

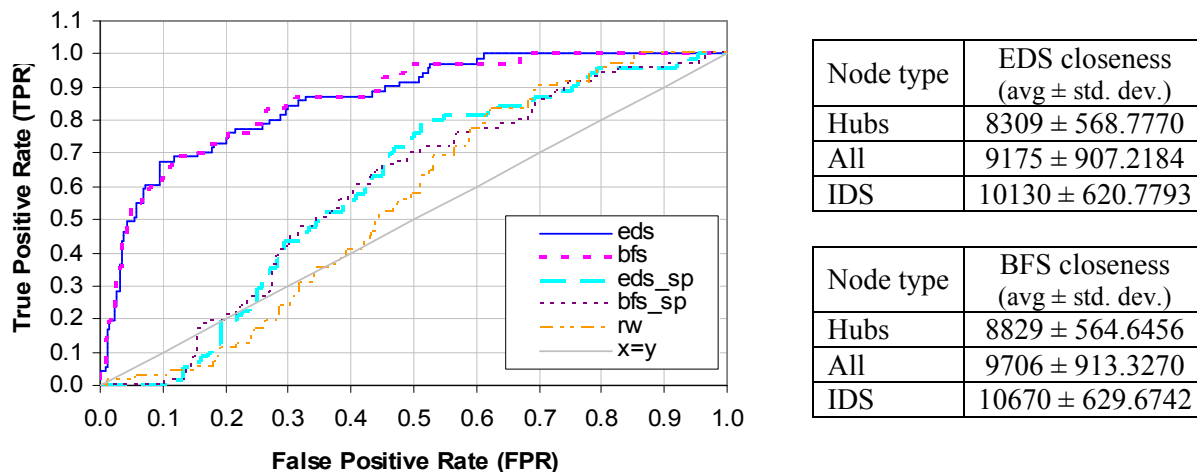


Fig. 12 Left: Recovery of the 71 hub residues using closeness based on estimated path commute time. Right: EDS and BFS closeness summary statistics for node by type. Hub nodes are PRN nodes that represent hub residues; IDS nodes are PRN nodes that represent IDS residues.

3.7 Identifying mutational hotspots

D816 is a mutational hotspot but not one of the 71 hub residues. Nor is it a hub in the conventional sense, i.e. its node degree is only 11 and 7/11 of its links are SE. In the WT PRN, node 816 ranks 98 by EDS closeness, and 115 by BFS closeness. (A node with a smaller closeness value has a smaller/higher closeness rank.) Of the seven mutational hotspots listed in section 2.6, only one (V654) is a hub residue. This suggests that a strategy different from both closeness based on estimated path commute time and node degree is needed for recovering or predicting mutational hotspots.

We noticed from our attempts to recover hub residues in section 3.6 that residues located next to a mutational hotspot in the KIT protein sequence tend to occupy highly central positions, i.e. have large *node betweenness*. Nodes that are traversed by many EDS or BFS paths have larger betweenness values. Therefore instead of trying to recover the seven mutational hotspots directly, we extended the target set to seven triples. Each triple comprises the hotspot residue and its immediate neighbors on the protein sequence. Our extended target set of residues is $\{(559, 560, 561), (653, 654, 655), (669, 670, 671), (815, 816, 817), (819, 820, 821), (821, 822, 823), (828, 829, 830)\}$. We need only recover one member from each triple to achieve 100% recovery.

Using this strategy of an extended target set and sorting the nodes in non-ascending order of their betweenness values, full recovery was possible with a False Positive Rate (FPR) of 26.54% (incurring the cost of 86 false positives). This best performance is yielded by EDS betweenness calculated using short-range paths only (*eds_sp* in Fig. 13). However, full recovery may not be necessary and the complete set of mutational hotspots may not be known *a priori*. At smaller FPRs, *eds_sp* also yielded the best performance. Small FPRs are preferably *per se*, but more so for this problem since there are potentially three tests associated with each candidate residue: the residue itself and its two sequence neighbors. This is where heuristics based on amino-acid chemistry and domain expertise can help further *in silico* winnowing of the candidates.

There are also qualitative differences in the order in which the mutational hotspot residues are recovered. The target residues and their respective ranks are listed in Table 7. Residues that neighbor 816 to its immediate left and right on the protein sequence (815 and 817) are easier to recover when all paths are used to compute node betweenness, i.e. *eds* and *bfs* columns in Table 7. We also note that 791, the left sequence neighbor of residue 792, which is mutated to restore communication interrupted by D816V, is

also ranked highly by both *eds* (rank 5) and *bfs* (rank 12). In contrast, residue 560, which borders IDS S2 in the JM-Switch region, and whose mutation is studied extensively in [14], is recovered most easily with *eds_sp*. This difference in effectiveness of short- and long-range paths may be a reflection of the difference in impact range of the mutational hotspots. While mutations at 816 produce long-range structural effects [2, 14], mutation at 560 did not appear to have a structural effect on the distant A-loop [14].

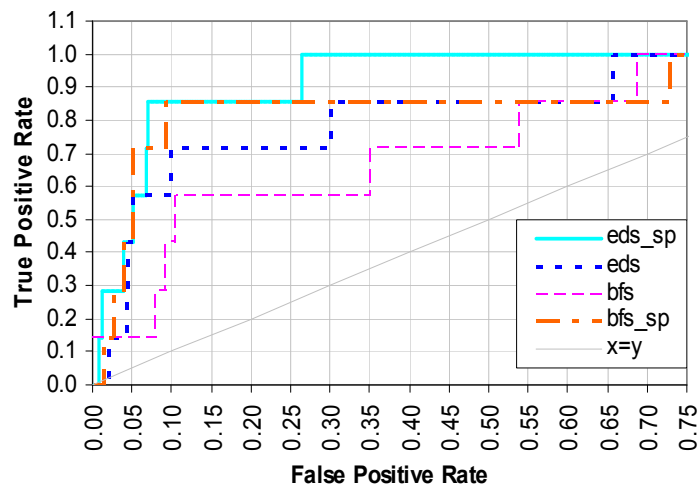
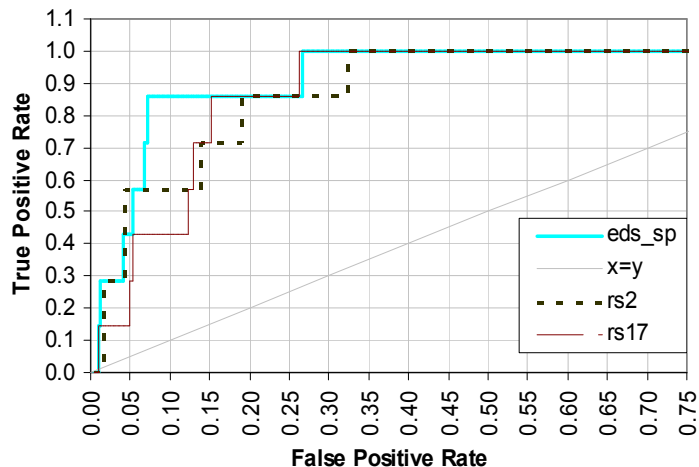


Fig. 13 Top: Recovery of the seven mutational hotspots using node betweenness based on EDS or BFS paths sorted in non-ascending order and an extended target set. Maximum number of false positives is $331 - 7 = 324$. Best performance (TPR = $6/7 = 85.71\%$; FPR = $23/324 = 7.10\%$) is achieved by *eds_sp* (node betweenness using only EDS SPs). SPs or short-range paths are paths whose source and target nodes are at most 10 sequence positions from each other (section 2.2).



Bottom: *eds_sp* outperforms random ordering of nodes. *rs2* and *rs17* are the two best results from 20 random node permutations.

For both EDS and BFS, node betweenness computed using short-range paths only, *eds_sp* and *bfs_sp* columns in Table 5, gave better results than node betweenness based on all paths (Fig. 13-top). We attribute this difference to the proximity of the mutational hotspots to IDSs. It may be that using only short-range paths to compute betweenness is helping to clarify the centrality of a node to the short-range communications around or within IDSs. IDSs by definition have highly independent dynamics. Residues of an IDS tend not to have long-range communications, preferring instead to a communication limit radius of four residues apart on the protein sequence [2]. Further, the residues of an IDS tend to be in sequence and the average size of an IDS is 10 (Table 1). Fittingly, the source and target nodes of short-range paths are at most 10 sequence positions apart (section 2.2). IDSs coincide with regulatory segments of KIT [2], in particular S2 and S8. S2 and S8 are of additional interest because they contain the phosphorylation sites Y568, Y570 and Y823. Thus, structural changes to IDSs can be expected to influence the modulation of KIT. A mutation at 560 significantly alters the structure of the JM-Switch region (S2) [14], while a mutation at 816 [2] perturbs both the JM-Switch and A-loop regions (S8) [2].

Table 7 Extended set of target mutational hotspot residues and their respective centrality rank. A more central residue has a larger betweenness value and a smaller/higher rank. Each bolded residue number increases the True Positive count by one to a maximum of seven.

<i>eds</i>		<i>eds sp</i>		<i>bfs</i>		<i>bfs sp</i>	
Rank	Residue	Rank	Residue	Rank	Residue	Rank	Residue
8	817	4	560	1	815	6	669
9	815	6	669	3	817	7	670
16	669	16	653	28	823	11	559
18	653	21	815	33	671	16	655
21	823	22	670	37	670	21	823
25	671	26	817	38	655	22	830
35	654	27	823	40	654	36	817
37	830	29	830	49	653	40	560
59	670	43	655	53	669	97	561
64	655	93	820	64	822	101	815
77	822	125	559	119	560	134	653
104	560	130	816	127	559	135	671
117	559	156	671	181	830	152	654
181	828	230	829	230	821	208	816
203	829	249	561	235	816	243	820
216	816	253	828	264	820	288	821
220	820	295	822	283	561	303	829
261	821	308	821	294	829	311	822
296	561	315	819	317	819	327	819
321	819	322	654	329	828	328	828

In contrast to the previous problem of recovering hub residues, the results produced with EDS betweenness for this task differs from the results produced with BFS betweenness. We attribute this divergence to increased problem difficulty. Compared to the hub recovery problem, the mutational hotspot recovery problem has fewer targets (7 vs. 71) in the same search space and therefore any difference in rank becomes more noticeable. With fewer needles in the haystack, we were concerned about the competitiveness of a random strategy, i.e. ranking the residues in random order. 20 permutations were generated and we report the best two in Fig. 13-bottom. Permutation *rs2* performed well at low FPRs, but took a long time to fully recover all targets. On the other hand, permutation *rs17* was slow to start but finished as quickly as *eds_sp*. It appears then that *eds_sp* gives the best of both worlds and is thus a better strategy than random.

4. Conclusion

We have shown that EDS paths on PRNs can give different outcomes from BFS paths on PRNs. These outcomes suggest that EDS paths make better models of intra-protein communication than BFS paths. On a set of 12 randomly selected proteins, EDS paths show themselves as significantly more stable and possessing significantly faster commute times than BFS paths. On the inactive form of KIT, running the EDS algorithm on WT PRN produced information in the form of shortcut edges and paths that proved more relevant than BFS paths for capturing the key features of KIT’s allosteric communication described in [2]. EDS was more effective than BFS at collecting residues of the KIT protein into meaningful clusters i.e. IDSs, and at locating segments in the KIT protein sequence where known mutational hotspots are present. A greater number of EDS paths connect the JMR to the A-loop region via the catalytic-loop, and these paths have faster estimated path commute time than the corresponding set of BFS paths. Communication between the IDS pair situated in the JMR and A-loop region (S1-S8) is also stronger with EDS than with BFS.

Acknowledgments

This work was made possible by the facilities of the Shared Hierarchical Academic Research Computing Network (SHARCNET:www.sharcnet.ca) and Compute/Calcul Canada. Thanks to the Dynameomics group for providing access to the MD data and to E. Laine for helpful discussions.

References

- 1 Morra G, Verkhivker G and Colombo G (2009) Modeling signal propagation mechanisms and ligand-based conformational dynamics of the Hsp90 molecular chaperone full-length dimer. *PLoS Comput Biol* 5(3):e1000323.
- 2 Laine E, Auclair C and Tchertanov L (2012) Allosteric communication across the native and mutated KIT Receptor Tyrosine Kinase. *PLoS Comput Biol* 8(8):e1002661.
- 3 Scarabelli G and Grant BJ (2013) Mapping the structural and dynamical features of kinesin motor domains. *PLoS Comput Biol* 9(11):e1003329.
- 4 Blacklock K and Verkhivker GM (2014) Computational modeling of allosteric regulation in the Hsp90 chaperones: A statistical ensemble analysis of protein structure networks and allosteric communications. *PLoS Comput Biol*; 10(6):e1003679.
- 5 Atilgan AR, Akan P and Baysal C (2004) Small-world communication of residues and significance for protein dynamics. *Biophysical Journal* 86:85-91.
- 6 Amitai G, Shemesh A, Sitbon E, Shklar M, Netanel D, Venger I and Pietrokovski S. (2004) Network analysis of protein structures identifies functional residues. *Journal of Molecular Biology* 344 1135-1146.
- 7 Park K and Kim D (2011) Modeling allosteric signal propagation using protein structure networks. *BMC Bioinformatics* 12. From The 9th Asia Pacific Bioinformatics Conference (APBC 2011) Incheon, Korea.
- 8 Khor S (2015) Protein residue networks from a local search perspective. *Journal of Complex Networks*. doi:10.1093/comnet/cnv014.
- 9 Kleinberg J (2000) Navigation in a small world. *Nature* 406:845.
- 10 Leitner DM (2008). Energy flow in proteins. *Annu. Rev. Phys. Chem.* 59:233-259.
- 11 Li G, Magana D and Dyer RB (2014) Anisotropic energy flow and allosteric ligand binding in albumin. *Nature Communications* 5:3100.
- 12 Greene LH and Higman VA (2003) Uncovering network systems within protein structures. *Journal of Molecular Biology* 334:781-791.
- 13 Liu H, Chen X, Focia PJ and He X (2007) Structural basis for stem cell factor-KIT signaling and activation of class III receptor tyrosine kinases. *EMBO J* 26:891-901.
- 14 Chauvot de Beauchene I *et al* (2014) Hotspot mutations in KIT receptor differentially modulate its allosterically coupled conformational dynamics: Impact on activation and drug sensitivity. *PLoS Comput. Biol.* 10(7):e1003749
- 15 Chatterjee S, Ghosh S and Vishveshwara, S (2013) Network properties of decoys and CASP predicted models: a comparison with native protein structures. *Mol. BioSyst.* 9:1774-1788.
- 16 Kannan N and Vishveshwara S (1999) Identification of side-chain clusters in protein structures by a graph spectral method. *J. Mol. Biol.* 292:441-464.
- 17 Humphrey W, Dalke A and Schulten K (1996) VMD - Visual Molecular Dynamics. *J. Molec. Graphics*, 14: 33-38. <http://www.ks.uiuc.edu/Research/vmd/>
- 18 Beck DAC, *et al.* (2008) Dynameomics: Mass Annotation of Protein Dynamics by All-Atom Molecular Dynamics Simulations. *Protein Engineering Design & Selection* 21: 353-368.
- 19 Van der Kamp MW *et al.* (2010) Dynameomics: A comprehensive database of protein dynamics. *Structure*, 18: 423-435.
- 20 Rosvall M and Bergstrom CT (2008) Maps of random walks on complex networks reveal community structure. *PNAS* 105(4):1118-1123.
- 21 S. van Dongen (2000) Graph clustering by flow simulation. PhD thesis, University of Utrecht.
- 22 van Dongen S and Abreu-Goodger C (2012) Using MCL to extract clusters from networks. *Methods*

- in Molecular Biology, 804:281-295.
- 23 Brohée S and van Helden J (2006) Evaluation of clustering algorithms for protein-protein interaction networks. BMC Bioinformatics 7:488.

Appendix A Pseudo-code for EDS

EDS(s, t)

Input: source node s , target node t , a graph G

Outputs: EDS path p //A sequence of nodes in order of EDS visit with s as the leftmost node and t as the rightmost node when EDS is successful.

$visited$ //The union of the set of nodes in p and their direct neighbors. The size of $visited$ is the cost of an EDS search.

Main variables: $inspected$ //The set of direct neighbors of nodes currently in p , excluding the nodes in p , sorted in ascending order by their Euclidean distance to t . The leftmost node of $inspected$ is a node currently closest to t and not already in p .

$level(x)$ //denotes the order node x is visited by EDS for the first time p .

```

1: append  $s$  to  $p$  //  $p = \langle s \rangle$ 
2: add  $s$  to  $visited$ 
3:  $level := 1$ ;  $level(s) := level$ 
4: do
5:    $x :=$  the rightmost node of  $p$ 
6:   for each node  $i$  in the set of direct neighbors of  $x$  in  $G$  do
7:     if  $i = t$  then
8:       append  $i$  to  $p$ 
9:       add  $i$  to  $visited$ 
10:       $level := level + 1$ ;  $level(i) := level$ 
11:      stop //path  $p$  from  $s$  to  $t$  is found
12:    end if
13:    if  $i$  is not in  $visited$  then
14:      add  $i$  to  $inspected$ 
15:    end if
16:  end for
17:  let  $y$  be the leftmost node in  $inspected$ 
18:  if  $x$  and  $y$  are linked in  $G$  then
19:    if there is a node  $z$  in  $p$  such that  $z \neq x$ , and  $z$  and  $y$  are linked in  $G$  then
20:      the edge  $(x, y)$  is a shortcut // $level(y) = level(x) + 1$ ;  $level(z) < level(x)$ 
21:    else //need to backtrack on  $p$  from  $x$  to reach  $y$ 
22:      inspect  $p$  from right to left starting at the rightmost node  $x$  for a node  $z$  that is a direct neighbor of  $y$ 
23:      append to  $p$  the sub-path of  $p$  starting from  $x$  to  $z$  // $p = \langle s \dots z \dots x \dots z \rangle$ 
24:    end if
25:    append  $y$  to  $p$ 
26:    add  $y$  to  $visited$ 
27:     $level := level + 1$ ;  $level(y) := level$ 
28:    remove  $y$  from  $inspected$ 
29:  while  $inspected$  is not empty
30: //path  $p$  from  $s$  to  $t$  is not found

```
